International Journal of Steel Structures
https://doi.org/10.1007/s13296-018-0053-7

A Fiber Model Based on Secondary Development of ABAQUS for Elastic–Plastic Analysis

Yan-Li Shi[1,2] · Hua-Wei Li[2] · Wen-Da Wang[2] · Chao Hou[3]

Received: 4 July 2017 / Accepted: 14 March 2018

Abstract
With the aim to provide an efficient platform for the elastic–plastic analysis of steel structures, reinforced concrete (RC) structures and steel–concrete composite structures, a program iFiberLUT based on the fiber model was developed within the framework of ABAQUS. This program contains an ABAQUS Fiber Generator which can automatically divide the beam and column cross sections into fiber sections, and a material library which includes several concrete and steel uniaxial material models. The range of applications of iFiberLUT is introduced and its feasibility is verified through previously reported test data of individual structural members as well as planar steel frames, RC frames and composite frames subjected to various loadings. The simulation results indicate that the developed program is able to achieve high calculation accuracy and favorable convergence within a wide range of applications.

Keywords Fiber model · Material constitutive model · Elastic–plastic analysis · Structure behavior

1 Introduction

As is known, experimental investigations at the structural system level are highly time-consuming and costly, because they require comparatively critical technical conditions. When the experimental techniques and facilities for structural system tests are limited, numerical analysis becomes an efficient choice to investigate the mechanical behavior of structures subjected to various loadings. There are two main modeling methods in a general-purpose finite element program, i.e., detailed three dimensional finite element model and fiber element model. The first one can be employed to achieve accurate numerical results, but building such models is tedious and calculation process is time-consuming for large structural systems under dynamic loadings (Katwal et al. 2017). Hence, with the pursuit of high-accuracy and efficiency in the analysis and design of practical structures, the fiber element model built on the material constitutive level has been increasingly adopted in structural nonlinear analysis (Lu et al. 2009).

In the fiber element model, beam and column cross sections are divided into a certain number of fibers. The geometric characteristics of a fiber are determined by its area and location with respect to the cross section (Taucer et al. 1991). Every fiber is then given non-linear uniaxial material properties which will eventually control the overall mechanical behavior of the cross section. During the element deformation process, the cross section is assumed to remain plane and perpendicular to the longitudinal axis of beams or columns. All strains and stresses of section fibers, meanwhile, are supposed to be parallel to the longitudinal axis. As the axial strains and stresses only combine axial forces and bending moments together, fiber models cannot take account of transverse shear effects of cross sections. It is a reasonable approximation to neglect the shear effects because most of structural beam and column members in practical structures have medium to large span over depth ratios (Spacone et al. 1996). The coupling influence of axial forces and bending moments on the mechanical behavior facilitate relatively high computational accuracy of the fiber model method (Wang et al. 2013; Tao and Nie 2014). Moreover, as the section fibers can be arranged flexibly along the cross section in the fiber model, structural beams and columns with

✉ Yan-Li Shi
ceshiyl@163.com

[1] School of Civil Engineering and Mechanics, Lanzhou University, Lanzhou 730000, People's Republic of China

[2] School of Civil Engineering, Lanzhou University of Technology, Lanzhou 730050, People's Republic of China

[3] School of Civil Engineering, The University of Sydney, Sydney, NSW 2006, Australia

Published online: 30 April 2018

different types of configurations can be analyzed expediently. A typical concrete filled steel tubular (CFST) column section is taken here as an example to illustrate the discretization of fibers along the cross section, as shown in Fig. 1. The CFST column section is divided into a different number of fibers based on the demands of computational accuracy. The uniaxial concrete or steel material models are then assigned to each corresponding fiber. The nonlinear behavior of this section derives entirely from the nonlinear stress–strain relation of the steel and concrete fibers. Moreover, it is worth mentioning that fiber model method cannot consider the bond-slip effect between steel and concrete fibers directly. Generally, a perfect bonding is assumed between different fibers. This assumption is suitable for steel–concrete composite structures (Wang et al. 2013). In contrast, for reinforcement concrete (RC) structure whose bond-slip deformations increase under seismic loadings, ignoring the bond-slip effect can cause certain calculation errors. However, if proper material models are employed for steel and concrete fibers, the bond-slip between them can be reflected equivalently in numerical analysis.

To date, the fiber model method has been implemented in quite a few programs for numerical analysis such as Perform-3D (CSI 2006), OpenSEES (Mazzoni et al. 2006), etc., but applications, operations and modeling processes in these programs have their own limitations. Perform-3D program, which aims in the analysis of structural seismic performance and nonlinear seismic design, does not have the universality for the numerical analysis of structural systems under other circumstances. OpenSEES possesses a high-performance solver, but it lacks visual preprocessor and postprocessor. It is inconvenience for users to build numerical models and to obtain visual results directly. In addition to Perform-3D and OpenSEES, Lu et al. (2008) developed a fiber model program named THUFIBER based on the secondary development interface of the general-purpose finite element program MSC.Marc. This program is suitable for nonlinear analysis of reinforced concrete structures under seismic loading and possesses high solution speed and accurate results (Lu et al. 2012). Comparatively, another general-purpose finite element software ABAQUS (ABAQUS 2010) possesses an accurate and efficient solver and provides various secondary development interfaces for users to customize specific requirements such as friendly graphical user interfaces to display simulation results. If the concept and the modeling method of fiber models are transplanted into ABAQUS through corresponding secondary development interfaces, the features of fiber models such as convenient modeling method and efficient calculation can be combined with the advantages of ABAQUS.

In this study, a fiber model program iFiberLUT has been developed based on the secondary development interfaces of ABAQUS. This program contains an ABAQUS Fiber Generator and a material library. The ABAQUS Fiber Generator can automatically divide the structural beam and column cross sections into fiber sections. The material library includes multiple concrete and steel uniaxial material models which are implemented by using the user-defined material (UMAT) mechanical behavior subroutine in ABAQUS. These typical concrete and steel material models are suitable for various analyzing cases such as monotonic and cyclic loadings in anti-collapse studies and seismic analyses. Take a numerical case as an example, the beam or column sections are divided into fibers based on the geometrical dimension of sections and computational accuracy by using the ABAQUS Fiber Generator. The rational uniaxial concrete or steel material models selected from the material library are assigned to each corresponding fiber. After specifying

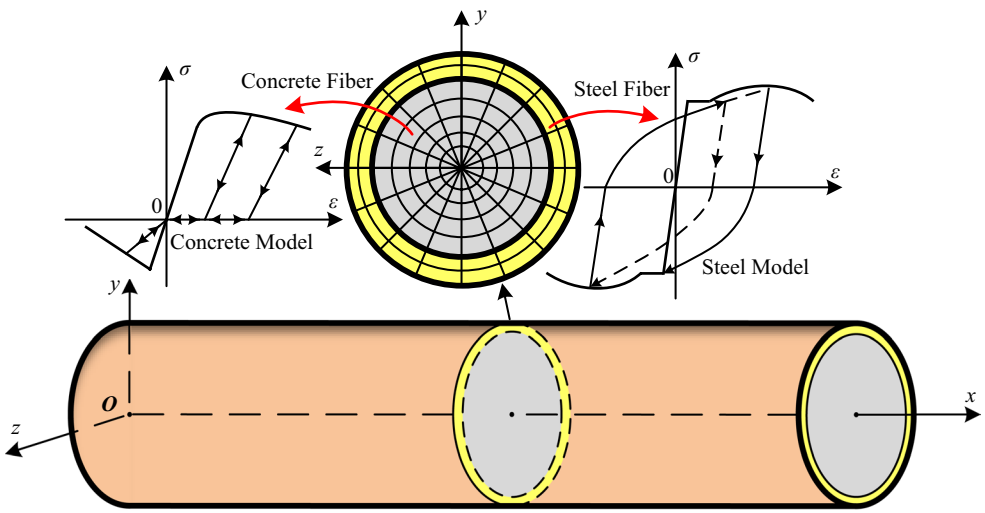

Fig. 1 Discretization of fibers along the cross section of CFST column

the loadings and boundary conditions of this specimen, the completed fiber model is then submitted to ABAQUS/Standard solver. The calculation result can be obtained visually in ABAQUS/CAE. Moreover, feasibility of the developed fiber model program is evaluated by comparing calculation results with test results from a serial of experiments of steel structures, reinforced concrete (RC) structures and steel–concrete composite structures subjected to various loadings. The results present that this program combining with ABAQUS solver can provide an efficient platform for numerical analysis.

2 ABAQUS Fiber Generator

To build the fiber element sections, the cross sections of beams and columns should be subdivided into many fibers. Three dimensional Timoshenko beam element provided in the element library of ABAQUS has the default layout of integration points, which can then be used as section fibers with nonlinear material behavior. By changing the number of integration points, the number of the section fiber layout can be modified flexibly. Moreover, the keyword "*rebar'' in ABAQUS can be used to define or add section fibers with different material properties.

In a fiber model of an engineering structure, beam and column sections possess numerous fibers, inducing relatively large workloads for subdivision of section fibers. In order to address this problem, the ABAQUS Fiber Generator developed hereby includes 6 basic section types and is able to automatically divide beam or column sections into a series of fibers. Figure 2 displays these 6 basic section types in ABAQUS Fiber Generator. Moreover, by assembling several basic section types, fiber subdivision of various complex sections can be conducted as well. After inputting the geometrical and material information of beam or column sections and the number of fibers in this program, the fiber information can be generated automatically and revised manually afterwards if modification is needed based on the users' judgement.

3 Material Library

The uniaxial constitutive models of different fiber materials play a critical role in fiber models to obtain accurate nonlinear responses of structural members (Tao and Nie

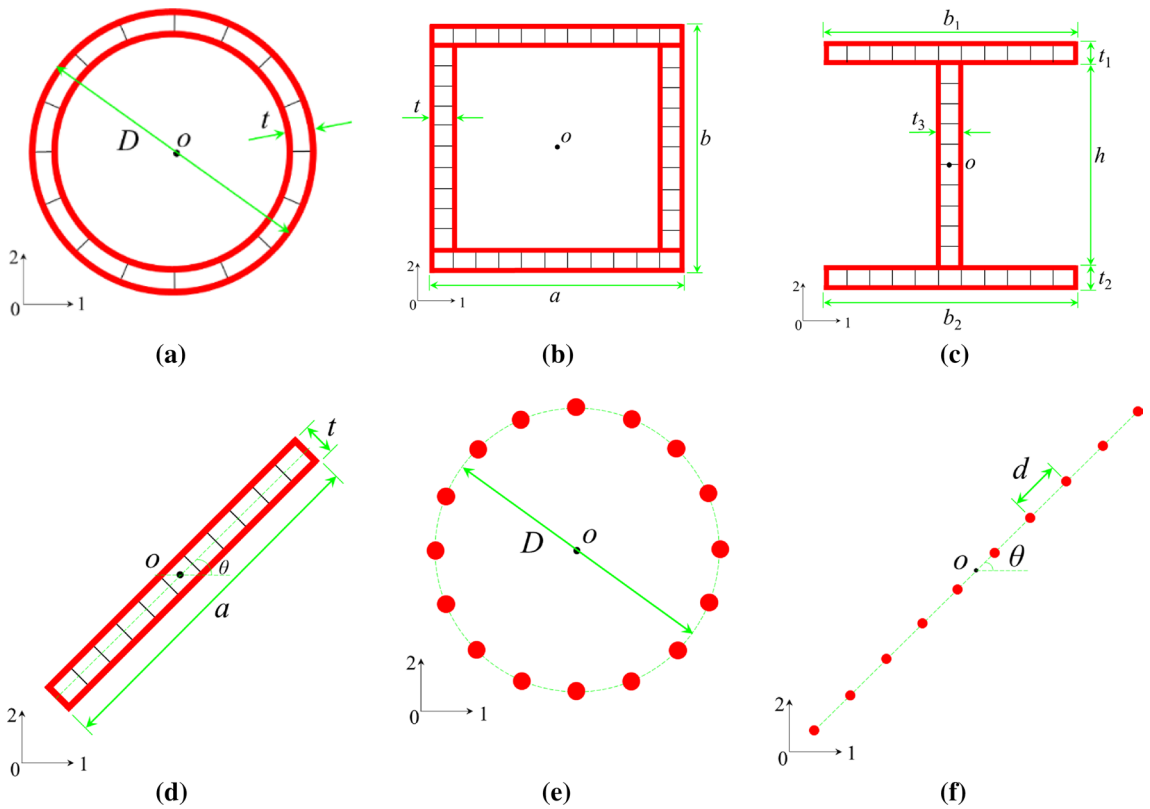

Fig. 2 Basic section types included in ABAQUS fiber generator. **a** Pipe section, **b** box section, **c** H-shaped section, **d** plate section, **e** rebar circle, **f** rebar row

2015). The rational material models should be selected for different structural types accordingly. However, various concrete and steel uniaxial constitutive models with different features are presented by some researchers now. It is confusing to decide which one should be used in numerical models. Besides, if all these material models are embedded into a fiber model program, it is an impractical and inefficient scheme. Thus, combining with several typical concrete and steel material constitutive models reported by previous researchers, the material library of iFiberLUT is developed based on the UMAT subroutine in ABAQUS (2010). This material library includes 5 typical constitutive models for concrete and another 5 for steel. Table 1 lists the concrete and steel uniaxial hysteresis constitutive models contained in the established material library, with their detailed characteristics introduced as follows.

3.1 iConcrete01 Model

The iConcrete01 model can be used for confined concrete in CFST members with circular cross sections. The uniaxial constitutive relation of the iConcrete01 model is displayed in Fig. 3. The compressive envelope curve was proposed by Han et al. (2007). The trend of this envelope curve is controlled by different confinement coefficient ξ, as shown in Fig. 3b. This coefficient reflects the stress-softening trend of the envelope curves. When ξ is greater than a critical value ξ_0, i.e., the concrete is well confined, the compressive envelope curve represents an upward trend and vice versa. By introducing the confinement coefficient ξ, the compressive envelope curve of the iConcrete01 model involves the confining effects of steel tubes on core concretes. The formula of ξ is expressed as Eq. (1), where A_s and A_c are the cross-sectional area of steel tube and concrete, respectively; f_y is the yield strength of steel and f_{ck} is the compressive strength of cuboid concrete (Han et al. 2007).

$$\xi = \frac{A_s f_y}{A_c f_{ck}} \tag{1}$$

The stress–strain relation of the compressive envelope curves in the iConcrete01 model is expressed as Eq. (2),

Table 1 Available constitutive models in iFiberLUT material library

Material model tag	Material model characteristic
iConcrete01	Confined concrete model for circular CFST members
iConcrete02	Confined concrete model for square and rectangular CFST members
iConcrete03	Concrete model in Chinese design guideline for concrete structures
iConcrete04	Scott–Kent–Park concrete model without tensile behavior
iConcrete05	Scott–Kent–Park concrete model with bilinear tensile behavior
iSteel01	Kinematic hardening bilinear steel model
iSteel02	Bilinear steel model with Clough's hysteretic rules
iSteel03	Esmaeily-Xiao steel model with Légeron's hysteretic rules
iSteel04	Esmaeily-Xiao steel model with Clough's hysteretic rules
iSteel05	Giuffré–Menegotto–Pinto steel model

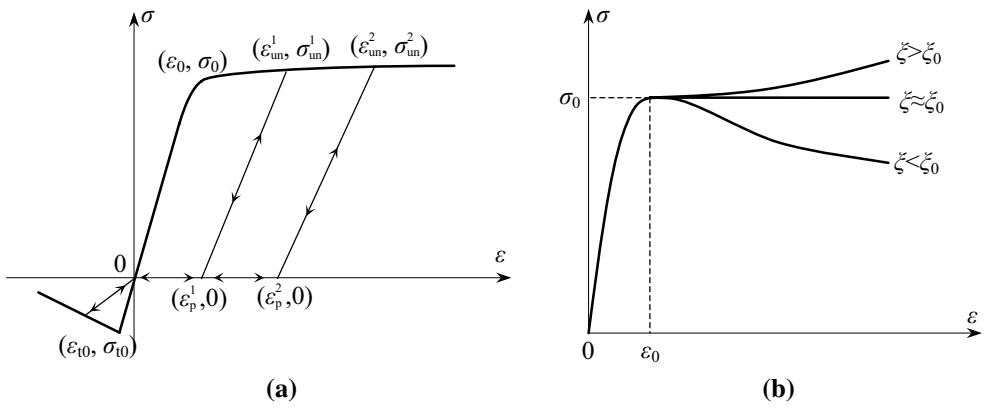

Fig. 3 Uniaxial constitutive relation of iConcrete01 model. **a** Uniaxial constitutive relation, **b** compression envelope curves with different confinement coefficient

in which f_c' represents the compressive strength of cylinder concrete.

$$y = \begin{cases} 2x - x^2 & (x \le 1) \\ \dfrac{1 + q \cdot (x^{0.1\xi} - 1)}{\beta \cdot (x-1)^2 + x} & \begin{matrix} (\xi \ge 1.12) \\ (\xi < 1.12) \end{matrix} \quad (x > 1) \end{cases} \tag{2}$$

where

$$x = \frac{\varepsilon}{\varepsilon_0}, \quad y = \frac{\sigma}{\sigma_0}$$

$$\sigma_0 = \left[1 + (-0.054 \cdot \xi^2 + 0.4 \cdot \xi) \cdot \left(\frac{24}{f_c'}\right)^{0.45}\right] \cdot f_c'$$

$$\varepsilon_0 = \varepsilon_{cc} + \left[1400 + 800 \cdot \left(\frac{f_c'}{24} - 1\right)\right] \cdot \xi^{0.2} \times 10^{-6}$$

$$\varepsilon_{cc} = (1300 + 12.5 f_c') \times 10^{-6}$$

$$q = \frac{\xi^{0.745}}{2 + \xi}$$

$$\beta = (2.36 \times 10^{-5})^{[0.25 + (\xi - 0.5)^7]} \times (f_c')^2 \times 3.51 \times 10^{-4}$$

A simplified formula based on the Mander model (Mander et al. 1988) for describing the hysteretic behavior of concrete is adopted as the cyclic unloading and reloading rules of concrete compression in the iConcrete01 model. As shown in Fig. 3a, straight lines are used in the unloading and reloading stages to indicate the compressive hysteretic rules. With the increase of the historical maximum compressive plastic strain, the residual plastic strain ε_p increase progressively and the unloading modulus is reduced gradually compared to the initial elastic modulus. The residual plastic strain ε_p after the unloading of compression force is determined based on Eq. (3) as follows,

$$\begin{cases} \varepsilon_p = \varepsilon_{un} - \dfrac{(\varepsilon_{un} + \varepsilon_{ca})\sigma_{un}}{\sigma_{un} + E_c \varepsilon_{ca}} \\ \varepsilon_{ca} = \max\left(\dfrac{\varepsilon_0}{\varepsilon_0 + \varepsilon_{un}}, \dfrac{0.09\varepsilon_{un}}{\varepsilon_0}\right)\sqrt{\varepsilon_0 \varepsilon_{un}} \end{cases} \tag{3}$$

where E_c is the initial elastic modulus of concrete; ε_{un} and σ_{un} are the strain and stress at the compressive unloading point, respectively; and ε_{c0} is the concrete strain at the peak strength.

In the unloading stage, after the compressive behavior is removed and only residual compressive strain is left, the concrete stress maintains zero until the concrete behavior turns into tension. Then in the reloading stage, the compressive reloading paths follow the latest unloading paths in the opposite direction.

The tensile behavior of the iConcrete01 model is displayed in Fig. 3a as well. The bilinear tension model is adopted. The elastic stage and tension softening stage are regarded as linear and σ_{t0} and ε_{t0} stand for the concrete tension strength and matching tension strain, respectively. The unloading and reloading paths of tension employ the secant modulus of the unloading point on the tension envelope curve.

3.2 iConcrete02 Model

The iConcrete02 model can be used for confined concrete in CFST members with square or rectangular sections. The trend of the compressive envelope curve, the compressive unloading and reloading behavior and tensile behavior are the same with the iConcrete01 model, but only the equation of compressive envelope curve is different due to the value of critical confined effect coefficient ξ_0. Thus, the uniaxial constitutive relation of the iConcrete02 model can be reflected by Fig. 3a as well. The compressive envelope curve in the iConcrete02 model is also proposed by Han et al. (2007) and expressed as Eq. (4), in which f_c' represents the compressive strength of cylinder concrete.

$$y = \begin{cases} 2x - x^2 & (x \le 1) \\ \dfrac{x}{\beta \cdot (x-1)^\eta + x} & (x > 1) \end{cases} \tag{4}$$

where

$$x = \frac{\varepsilon}{\varepsilon_0}, \quad y = \frac{\sigma}{\sigma_0}$$

$$\sigma_0 = \left[1 + (-0.0135 \cdot \xi^2 + 0.1 \cdot \xi) \cdot \left(\frac{24}{f_c'}\right)^{0.45}\right] \cdot f_c'$$

$$\varepsilon_0 = \varepsilon_{cc} + \left[1330 + 760 \cdot \left(\frac{f_c'}{24} - 1\right)\right] \cdot \xi^{0.2} \times 10^{-6}$$

$$\varepsilon_{cc} = (1300 + 12.5 f_c') \times 10^{-6}$$

$$\eta = 1.6 + 1.5/x$$

$$\beta = \begin{cases} \dfrac{(f_c')^{0.1}}{1.35\sqrt{1+\xi}} & (\xi \le 3.0) \\ \dfrac{(f_c')^{0.1}}{1.35\sqrt{1+\xi \cdot (\xi-2)^2}} & (\xi > 3.0) \end{cases}$$

3.3 iConcrete03 Model

The iConcrete03 model employs the concrete model in the Chines design guideline for concrete structures GB50010 (2010). The uniaxial constitutive relation of the iConcrete03

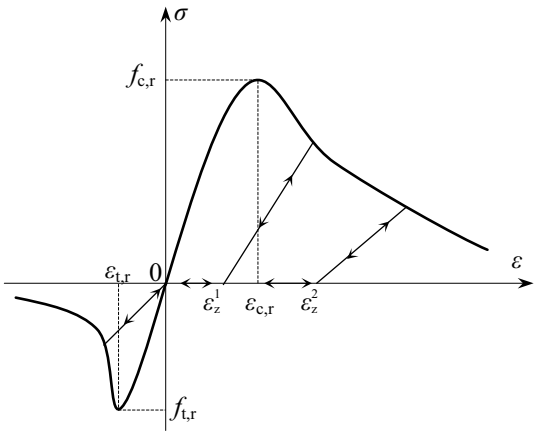

Fig. 4 Uniaxial constitutive relation of iConcrete03 model

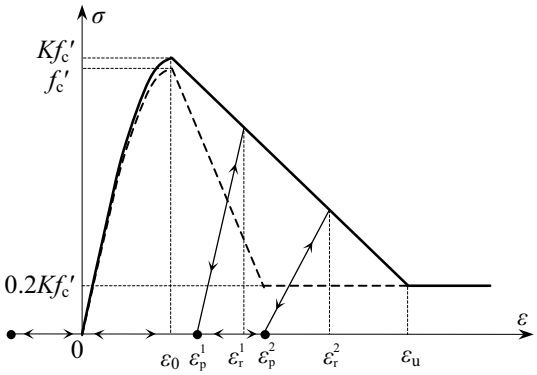

Fig. 5 Uniaxial constitutive relation of iConcrete04 model

model is shown in Fig. 4. Compressive and tensile envelope curves of this model are controlled by uniaxial damage evolution parameter. By adjusting the parameter value of decline stage, the decreasing amplitude can be controlled to illustrate the damaged degree of concrete strength. Formula of the compressive envelope curve is illustrated as Eq. (5), where E_c is the concrete initial elastic modulus, $f_{c,r}$ is the uniaxial compressive strength of cuboid concrete, $\varepsilon_{c,r}$ is the strain corresponding to $f_{c,r}$, d_c is the compressive uniaxial damage evolution parameter, and α_c is a compressive parameter to control the compressive decline curve shape.

$$\sigma = (1 - d_c)E_c\varepsilon \tag{5a}$$

$$d_c = \begin{cases} 1 - \frac{\rho_c n}{n-1+x^n} & x \le 1 \\ 1 - \frac{\rho_c}{\alpha_c(x-1)^2+x} & x > 1 \end{cases} \tag{5b}$$

$$\alpha_c = 0.157 f_{c,r}^{0.785} - 0.905 \tag{5c}$$

$$\rho_c = \frac{f_{c,r}}{E_c\varepsilon_{c,r}} \tag{5d}$$

$$n = \frac{E_c\varepsilon_{c,r}}{E_c\varepsilon_{c,r} - f_{c,r}} \tag{5e}$$

$$x = \frac{\varepsilon}{\varepsilon_{c,r}} \tag{5f}$$

The tensile envelope curve is expressed as Eq. (6), where $f_{t,r}$ is the uniaxial tensile strength of cuboid concrete, $\varepsilon_{t,r}$ is the strain corresponding to $f_{t,r}$, d_t is the tensile uniaxial damage evolution parameter, and α_t is a tensile parameter to control the tensile decline curve shape.

$$\sigma = (1 - d_t)E_c\varepsilon \tag{6a}$$

$$d_t = \begin{cases} 1 - \rho_t(1.2 - 0.2x^5) & x \le 1 \\ 1 - \frac{\rho_t}{\alpha_t(x-1)^{1.7}+x} & x > 1 \end{cases} \tag{6b}$$

$$\alpha_t = 0.312 f_{t,r}^2 \tag{6c}$$

$$\rho_t = \frac{f_{t,r}}{E_c\varepsilon_{t,r}} \tag{6d}$$

$$x = \frac{\varepsilon}{\varepsilon_{t,r}} \tag{6e}$$

Similar to the hysteretic rules of the iConcrete01 and the iConcrete02 models, the simplified Mander model is also employed in the compressive and tensile unloading and reloading criteria of the iConcrete03 model.

3.4 iConcrete04 Model

The iConcrete04 model considers the stirrup confinement effect on concrete and neglects the tensile behavior of concrete. This model was first used in Taucer's research (Taucer et al. 1991). Figure 5 shows the uniaxial constitutive relation of the iConcrete04 model. The monotonic envelope curve of this concrete model follows the modified Kent and Park model which was initially put forward by Kent and Park (1971) and then extended by Scott et al. (1982). The monotonic concrete stress–strain relation in compression is described as Eq. (7).

$$\sigma = \begin{cases} Kf_c'\left[2\left(\frac{\varepsilon}{\varepsilon_0}\right) - \left(\frac{\varepsilon}{\varepsilon_0}\right)^2\right] & (\varepsilon \le \varepsilon_0) \\ Kf_c'\left[1 - Z(\varepsilon - \varepsilon_0)\right] & (\varepsilon_0 < \varepsilon \le \varepsilon_u) \\ 0.2Kf_c' & (\varepsilon > \varepsilon_u) \end{cases} \tag{7}$$

where

$$\sigma_0 = Kf_c', \quad \varepsilon_0 = 0.002K$$

$$K = 1 + \frac{\rho_s f_{yh}}{f_c'}$$

$$Z = \frac{0.5}{\frac{3+0.29f_c'}{145f_c'-1000} + 0.75\rho_s\sqrt{\frac{h'}{s_h}} - 0.002K}$$

$$\varepsilon_u = 0.004 + 0.9\rho_s\left(\frac{f_{yh}}{300}\right) \quad \text{or} \quad \varepsilon_u = \varepsilon_0 + \frac{0.8}{Z}$$

f_c' is the compressive strength of cylinder concrete, ε_0 is the concrete strain at maximum stress, ε_u is the concrete strain at 20% of maximum stress, K is a factor which represents the increase of compressive strength due to stirrup confinement, ρ_s is the ratio of the volume of hoop reinforcement to the volume of concrete core measured over the outer surface of stirrups, f_{yh} is the yield strength of stirrups, Z is the strain softening slope, h' is the width of concrete core measured to the outer surface of stirrups, and s_h is the center spacing of stirrups or hoop sets.

The cyclic unloading and reloading rules suggested by Karsan and Jirsa (Karsan and Jirsa 1969) are approved as the hysteresis behavior of the concrete stress–strain relation in the compressive region. The concrete degradation degree of stiffness is reflected by the decrease of the unloading line slope. When concrete unloading behavior occurs, stain-stress relation follows the unloading line to the point of the residual plastic strain ε_p at the strain axis, then the concrete stress stays zero as the iConcrete04 model does not consider the tensile behavior. The reloading behavior follows the latest unloading path in the opposite direction. The residual plastic strain ε_p in compressive unloading behavior is calculated by Eq. (8), where ε_r is the strain of the unloading point at the monotonic envelope curve.

$$\begin{aligned} \frac{\varepsilon_p}{\varepsilon_0} &= 0.145\left(\frac{\varepsilon_r}{\varepsilon_0}\right)^2 + 0.13\left(\frac{\varepsilon_r}{\varepsilon_0}\right)\left(\frac{\varepsilon_r}{\varepsilon_0}\right) < 2 \\ \frac{\varepsilon_p}{\varepsilon_0} &= 0.707\left(\frac{\varepsilon_r}{\varepsilon_0} - 2\right) + 0.834\left(\frac{\varepsilon_r}{\varepsilon_0}\right) \geq 2 \end{aligned} \tag{8}$$

3.5 iConcrete05 Model

The iConcrete05 model is the Scott–Kent–Park concrete model with bilinear tensile behavior. The compressive monotonic envelope curve of this model, employing the modified Kent and Park model (Kent and Park 1971; Scott et al. 1982), is the same as that of iConcrete04 model. However, the cyclic unloading and reloading behavior represented by Yassin (1994) is adopted in this model. Moreover, the iConcrete05 model considers the bilinear tensile behavior to reflect the tensile capacity of concrete. Figure 6 exhibits the uniaxial constitutive relation of this model.

In the compressive region, with the increasing of the values of maximum strain, a successive degradation of stiffness of both the unloading and reloading lines occurs. The degradation degree of stiffness is controlled by the intersection point R of the tangent to the compressive monotonic envelop curve at the origin and the unloading line from point B that corresponds to a certain concrete strength value (20% of maximum stress) in Fig. 6a. When the point R is determined, all the reloading lines will intersect at this point. The strain and stress at the intersection point R is expressed as Eq. (9),

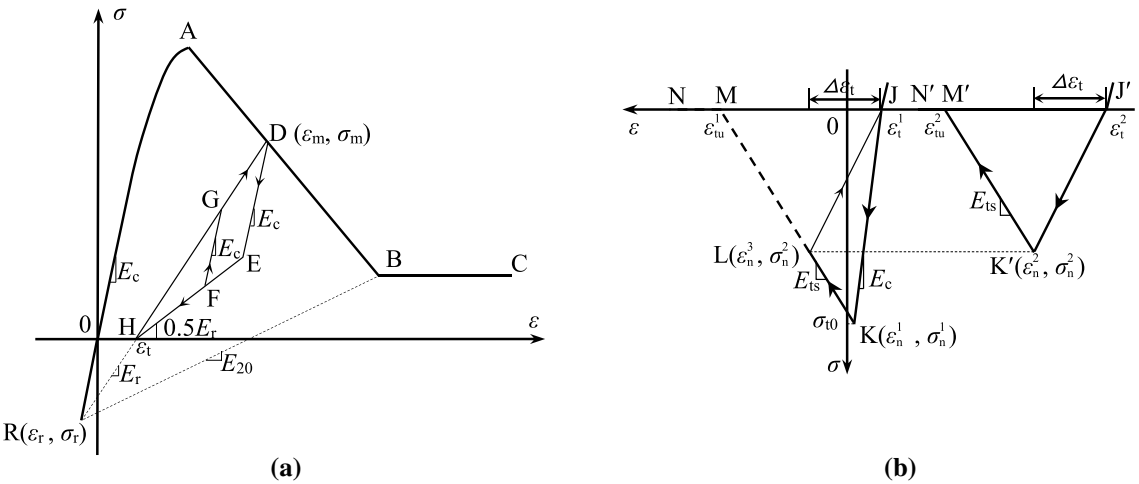

Fig. 6 Uniaxial constitutive relation of iConcrete05 model. **a** Uniaxial compressive relation, **b** uniaxial tensile relation

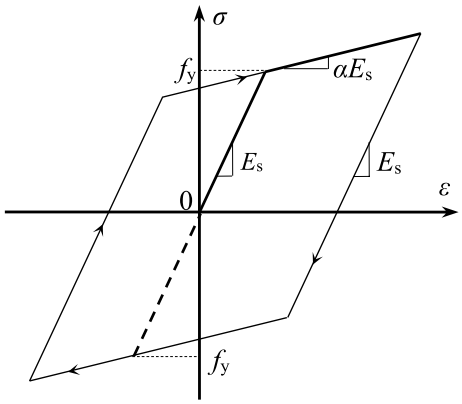

Fig. 7 Uniaxial constitutive relation of iSteel01 model

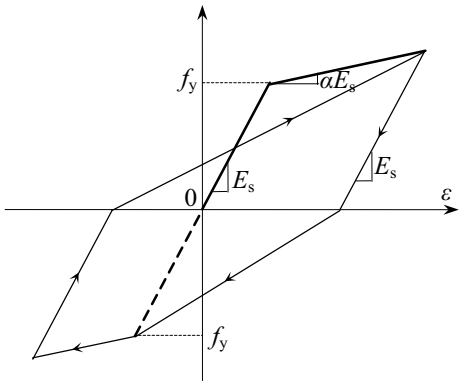

Fig. 8 Uniaxial constitutive relation of iSteel02 model

where E_c is the tangent modulus of the monotonic envelope curve at the origin, E_{20} is the reloading modulus at point B.

$$\begin{aligned}\varepsilon_r &= \frac{0.2Kf_c' - E_{20}\varepsilon_{20}}{E_c - E_{20}}\\ \sigma_r &= E_c\varepsilon_r\\ E_c &= \frac{2Kf_c'}{\varepsilon_0}\end{aligned} \tag{9}$$

The cyclic unloading and reloading relations pass several points which define the hysteretic loop such as DEFHGD or DEFGD in Fig. 6a. Point H is the compressive residual plastic strain point which also stands for the starting point of the tensile behavior (like point J or J′ in Fig. 6b).

The uniaxial tensile relation of the iConcrete05 model is shown in Fig. 6b. When hysteretic behavior occurs in the tensile region, the unloading or reloading lines link the unloading points and the origin or the last compressive residual strain points, such as line LJ or J′K′ in Fig. 6b. When the tensile stress drops to zero, it remains zero with the increasing of strain (line MN or M′N′), indicating that the concrete tensile capacity is depleted.

3.6 iSteel01 Model

The iSteel01 model is the classic kinematic hardening bilinear steel model. By adjusting the hardening coefficient α, this model can be used in steel models with various hardening degree such as the ideal elastic–plastic model. Figure 7 displays the uniaxial constitutive relation of the iSteel01 model, where E_s is the steel elasticity modulus and f_y is the yield strength of steel.

3.7 iSteel02 Model

The iSteel02 model is a bilinear steel model with Clough's unloading and reloading rules, as shown in Fig. 8. The monotonic envelope curves of the iSteel02 model are bilinear and the hysteretic behavior bases on the maximum history strain point oriented criterion proposed by Clough and Johnston (1966). In this hysteretic rule, the unloading modulus equals to the steel elasticity modulus E_s, and reloading lines point to the maximum history strain of the opposite mechanical behavior. Moreover, the characteristics of this hysteretic rule are conducive to compensating the disadvantage of the fiber model which cannot reflect the bond-slip effect between steel and concrete fibers.

3.8 iSteel03 Model

The iSteel03 model was proposed by Wang et al. (2007), which combines the monotonic envelope curves proposed by Esmaeily and Xiao (2005) with the Légeron's hysteretic model (Légeron et al. 2005). Figure 9 shows the uniaxial constitutive relation of the iSteel03 model.

The iSteel03 model can regulate the shape of the monotonic envelope curves by importing three parameters k_1, k_2, k_3. Equation (10) illustrates the formula for the monotonic envelope curves and Fig. 9b, c display the monotonic stress–strain relation with or without an evident yield stage, respectively.

$$\sigma = \begin{cases} E_s\varepsilon & (\varepsilon \le \varepsilon_y)\\ f_y & (\varepsilon_y < \varepsilon \le k_1\varepsilon y)\\ k_3 f_y + \frac{E_s(1-k_3)}{\varepsilon_y(k_2-k_1)^2}(\varepsilon - k_2\varepsilon_y)^2 & (\varepsilon > k_1\varepsilon_y)\end{cases} \tag{10}$$

where E_s is the steel elasticity modulus, f_y and ε_y are the yield stress and strain respectively, k_1 is the ratio of the strain corresponding to the start point of the hardening stage over the yield strain, k_2 is the ratio of the strain corresponding to

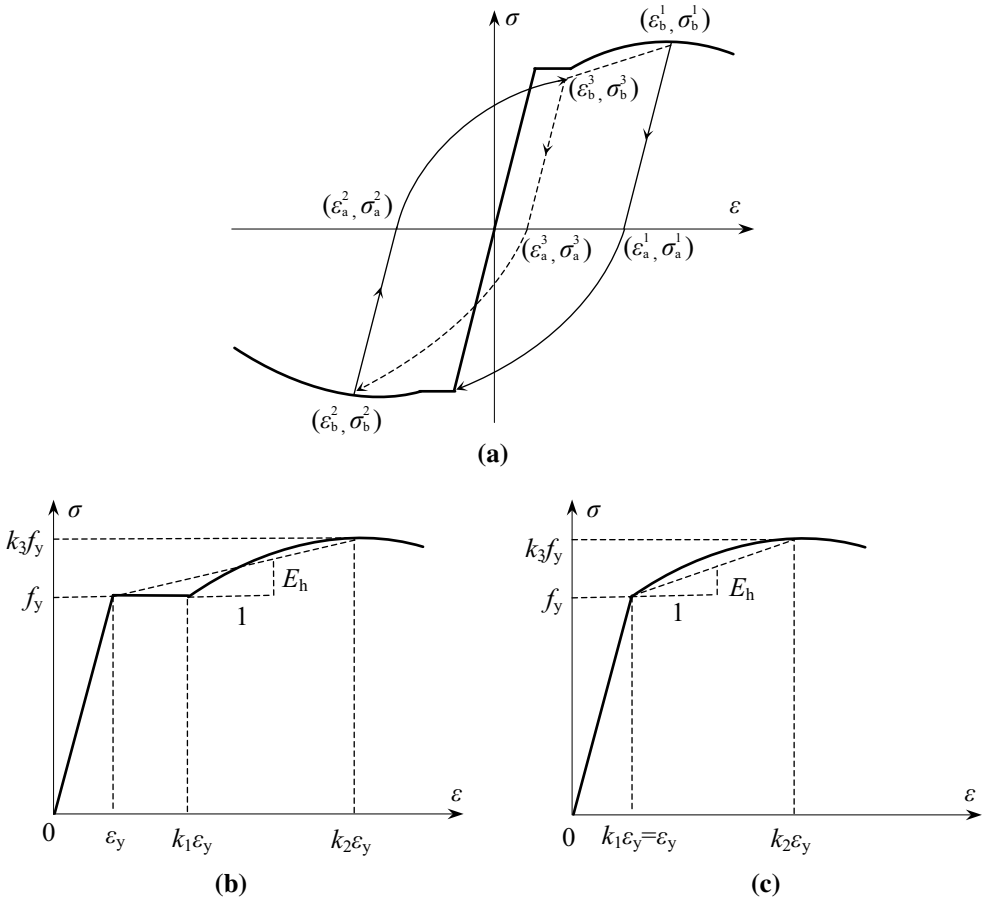

Fig. 9 Uniaxial constitutive relation of iSteel03 model. **a** Uniaxial constitutive relation, **b** monotonic envelope curves with a yield stage, **c** monotonic envelope curves without a yield stage

the peak stress over the yield strain, k_3 is the ratio of peak stress over the yield stress.

When $k_1 = 1$, the monotonic envelope curves do not possess a yield stage in Fig. 9c. Moreover, this model adopts a parameter k_4, the ratio of the tensile yield stress over the compressive yield stress, to reflect the mechanical behavior of high-strength steel rebar with unequal yield strength of the tensile and compressive behavior.

The Légeron's hysteretic model (Légeron et al. 2005) is employed in the unloading and reloading rules of the iConcrete03 model, as shown in Fig. 9a. The unloading modulus is assumed to be equal to the elasticity modulus. The Bauschinger effect can be vividly reflected by the curved reloading path which links the start point of reverse reloading path (i.e. the unloading point at the monotonic envelope curves) and the maximum history strain point in the opposite direction. Equation (11) illustrates the formula of the reloading path curves.

$$\sigma = \left[E_s(\varepsilon - \varepsilon_a) + \sigma_a\right] - \left[E_s(\varepsilon_b - \varepsilon_a) - (\sigma_b - \sigma_a)\right]\left[\frac{\varepsilon - \varepsilon_a}{\varepsilon_b - \varepsilon_a}\right]^p$$
$$p = \frac{(E_s - E_h)(\varepsilon_b - \varepsilon_a)}{E_s(\varepsilon_b - \varepsilon_a) - (\sigma_b - \sigma_a)} \tag{11}$$

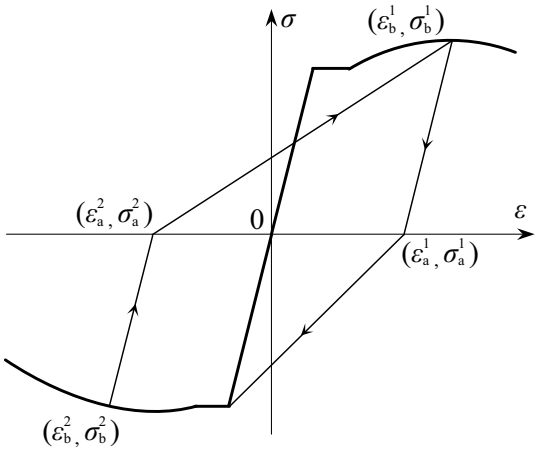

Fig. 10 Uniaxial constitutive relation of iSteel04 model

where E_h is the equivalent hardening modulus showed in Fig. 9b, σ_a and ε_a are the stress and strain at the reverse start point of reloading path respectively; σ_b and ε_b are the stress and strain at the unloading point, respectively.

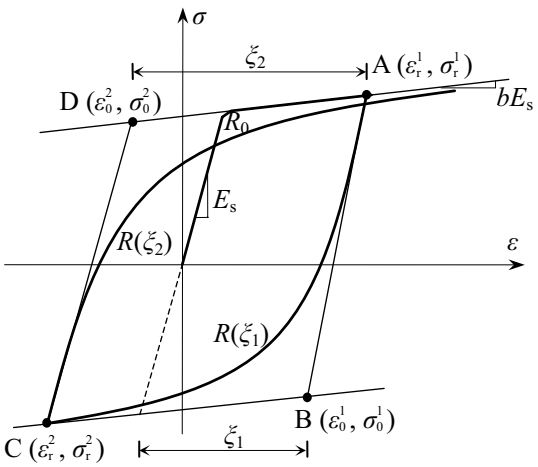

Fig. 11 Uniaxial constitutive relation of iSteel05 model

3.9 iSteel04 Model

The iSteel04 model combines the monotonic strain–stress relation proposed by Esmaeily and Xiao (2005) with Clough's unloading and reloading rules (Clough and Johnston 1966). Figure 10 shows the uniaxial constitutive relation of the iSteel04 model. This model takes the advantage of the general applicability of the monotonic envelope curves as described in the iSteel03 model. Instead of the Légeron's hysteretic model in the iSteel03 model, the Clough's hysteretic rules which can roughly reflect the bond-slip effect between steel and concrete fibers is employed in the iSteel04 model.

3.10 iSteel05 Model

The iSteel05 model follows the Giuffré–Menegotto–Pinto model, which is initially proposed by Giuffré and Pinto (1970), later improved by Menegotto and Pinto (1973), and added isotropic strain hardening by Filippou et al. (1983). Figure 11 shows the stress–strain relation of the iSteel05 model. Equation (12) expresses the formula of this model.

$$\sigma^* = b\varepsilon^* + \frac{(1-b)\varepsilon^*}{(1+\varepsilon^{*R})^{1/R}} \tag{12a}$$

where

$$\varepsilon^* = \frac{\varepsilon - \varepsilon_r}{\varepsilon_0 - \varepsilon_r} \tag{12b}$$

$$\sigma^* = \frac{\sigma - \sigma_r}{\sigma_0 - \sigma_r} \tag{12c}$$

$$R = R_0 - \frac{R_1 \xi}{R_2 + \xi} \tag{12d}$$

and

$$\xi = \left| \frac{\varepsilon_m - \varepsilon_0}{\varepsilon_y} \right| \tag{12e}$$

The unloading and reloading paths are represented by a curved transition from a straight line asymptote with slope E_s (line AB or CD in Fig. 11) to another asymptote with slope bE_s (line BC or DA in Fig. 11). In this figure, σ_r and ε_r are the stress and strain at the strain reversal point (Point A and C in Fig. 11), σ_0 and ε_0 are the stress and strain at the intersection point of two asymptotes (point B and D in Fig. 11), b is the hardening coefficient, and R is a parameter that influences the curvature of the transition curve between the two asymptotes, which controls a good representation of the Bauschinger effect.

4 Verification of the iFiberLUT Program

For a newly developed program, it should be verified and calibrated by existing test cases because it is critical to ensure the accuracy and efficiency of this program in numerical analysis. Typical experimental investigations of steel structures, RC structures and steel–concrete composite structures reported by other researchers are adopted to demonstrate the ability of the developed fiber model program iFiberLUT. The cross sections of beams and columns are divided into fibers by using the ABAQUS Fiber Generator. Since the nonlinear behavior of these specimens derives from the accuracy and validity of fiber material models, rational concrete and steel material models are selected from the material library described above. The geometry, material and loading information of specimens and the test and numerical results of various structures are illustrated as follows.

4.1 Steel Structures

Wu et al. (2006) studied the seismic capacity of a planar steel frame in 1/2 scale under horizontal cyclic loading. Figure 12a shows the geometry, material and loading information of this steel frame. Corresponding numerical model is established by using iFiberLUT and the iSteel04 model is adopted for the steel material. The calculated and experimental horizontal force versus displacement curves are illustrated and compared in Fig. 12b. As can be seen, the numerical result is consistent with the experimental result, which indicates that this developed fiber model program gives reliable predication of the mechanical behavior of steel frames under cyclic loading.

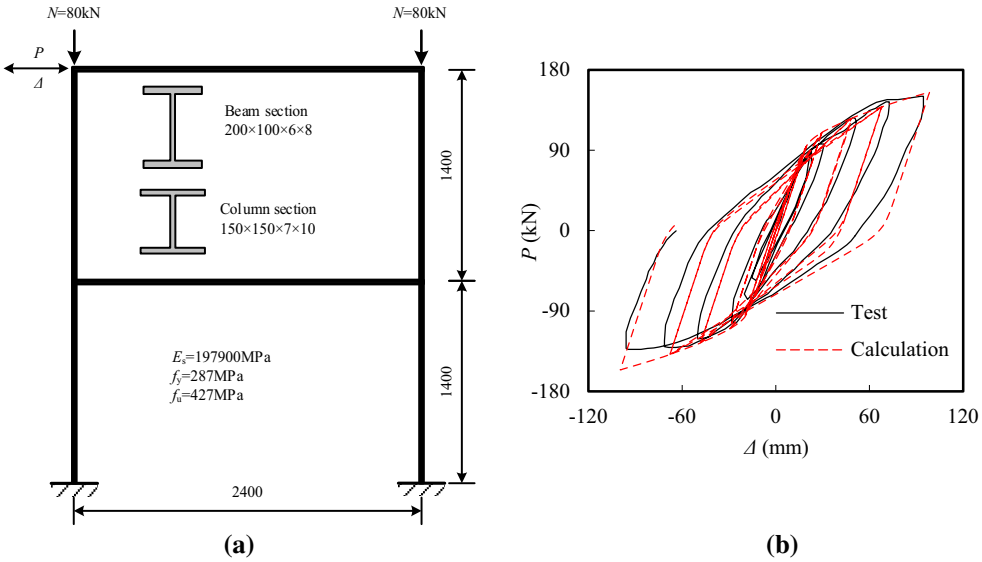

Fig. 12 Verification of steel frame under horizontal cyclic load. **a** Information of steel frame, **b** comparison results of steel frame

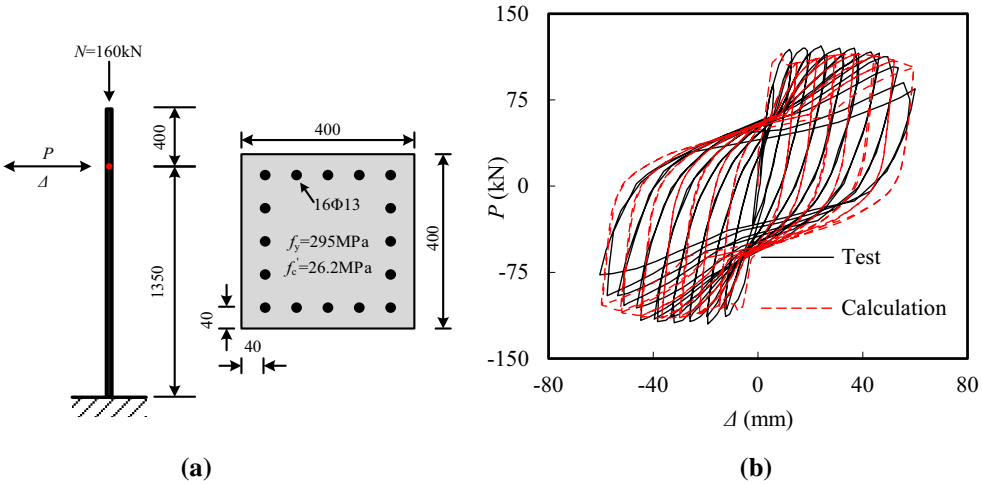

Fig. 13 Verification of RC column under horizontal cyclic load. **a** Information of RC column, **b** comparison results of RC column

4.2 Reinforced Concrete Structures

Kawashima et al. (2004) reported a series of tests on RC bridge columns subjected to cyclic loading. One of the specimens under unilateral cyclic loading is selected for verifying the numerical model. The essential geometry, material and loading information of this specimen are displayed in Fig. 13a. The iConcrete05 model and the iSteel03 model are, respectively, applied for the concrete and steel bars. Close agreement between the calculation and test results can be obtained in Fig. 13b. It can be seen that the degradation of strength and stiffness of RC columns can be reasonably predicted in the fiber model.

Two 3-story planar RC frames subjected to cyclic loading were tested by Zou and Zhou (2005). In regard to the material strength of these two frames, the corresponding yield strength of rebar for ϕ12 and ϕ14 are 343.8 and 349.5 MPa and the compressive strength of cubic concrete for the first, second and top floor are 39.6, 40.7 and 45.3 MPa, respectively. Figure 14a, b exhibit the geometry and loading information of these two RC frames. For frame 1, the vertical loads are applied on the top of the two side columns while the iConcrete04 model and the iSteel02 model are correspondingly chosen for the concrete and rebar. However, for frame 2, the vertical loads are applied on the top of the two side columns as well as the midpoint of the top beam, while the concrete and rebar employ the iConcrete05 model and the iSteel04 model, respectively. The horizontal force versus displacement curve of the calculation result agrees well with that from the experiments, as shown in Fig. 14c, d. Since the hysteretic rule of the iSteel02 and iSteel04 models are conducive to compensating the bond-slip effect between steel and concrete fibers, the developed fiber model program represents reasonable predictions of the stiffness

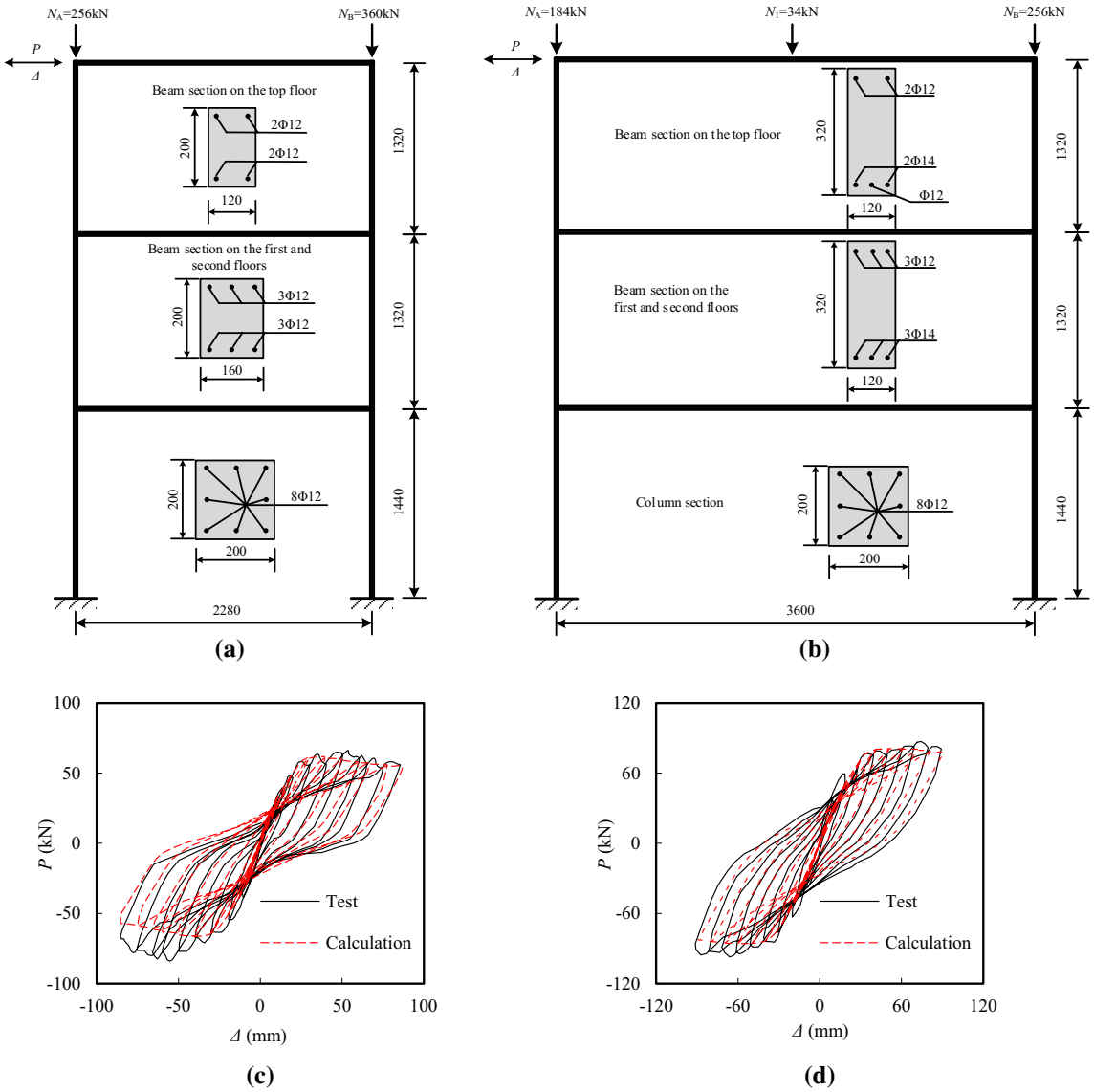

Fig. 14 Verification of RC frames under horizontal cyclic load. **a** Information of RC frame 1, **b** information of RC frame 2, **c** comparison results of RC frame 1, **d** comparison results of RC frame 2

degradation of RC structures. Besides, the results show that the bond-slip effect between steel and concrete fibers can be reflected equivalently by using proper material models in RC structures.

In order to investigate the performance of RC frames against progressive collapse, Yi et al. (2008) tested a 3-story and 4-bay 1/3 scale planar RC frame under a column removal scenario. Information of this RC frame is shown in Fig. 15a. The iConcrete03 model and the iSteel05 model are adopted for the concrete and rebar, respectively. The relation of vertical force and displacement at the location of the failure column indicates the capacity of this RC frames to resist collapse. As illustrated in Fig. 15b, the fiber element model built by iFiberLUT accurately estimates the performance in terms of load-carrying capacity and residual displacement.

4.3 Steel–Concrete Composite Structures

The mechanical behavior of CFST columns under axial compression has been studied by Hu et al. (2003). A circular section specimen labelled as CU-40 is chosen for the verification with its information shown in Fig. 16a. The core concrete and steel tube employ the iConcrete01 model and the iSteel01 model, respectively. The axial force versus strain curve simulated by iFiberLUT matches the test result well both in stiffness and loading capacity, as represented in Fig. 16b.

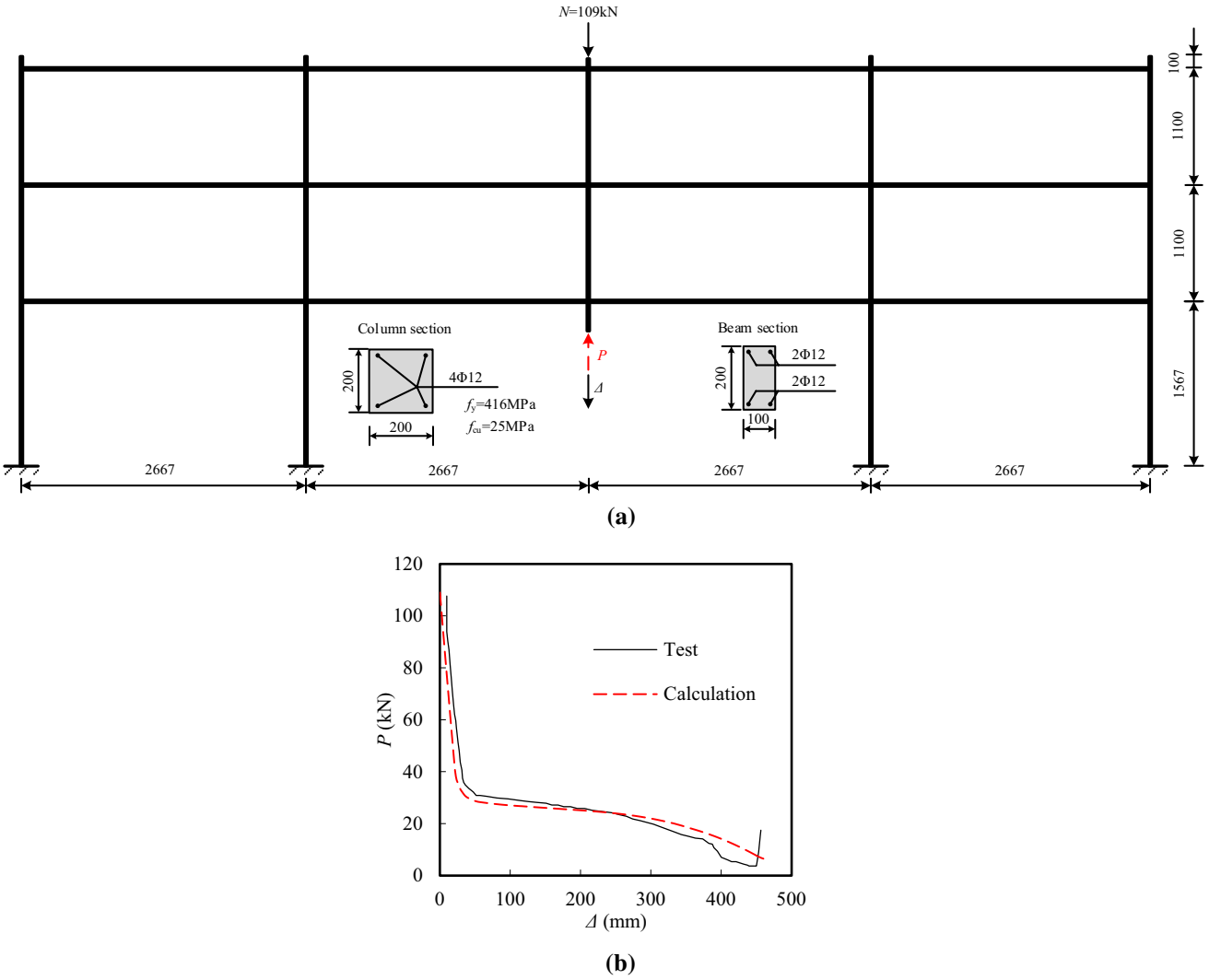

Fig. 15 Verification of RC frame under a column removal scenario. **a** Information of RC frame, **b** comparison results of RC frame

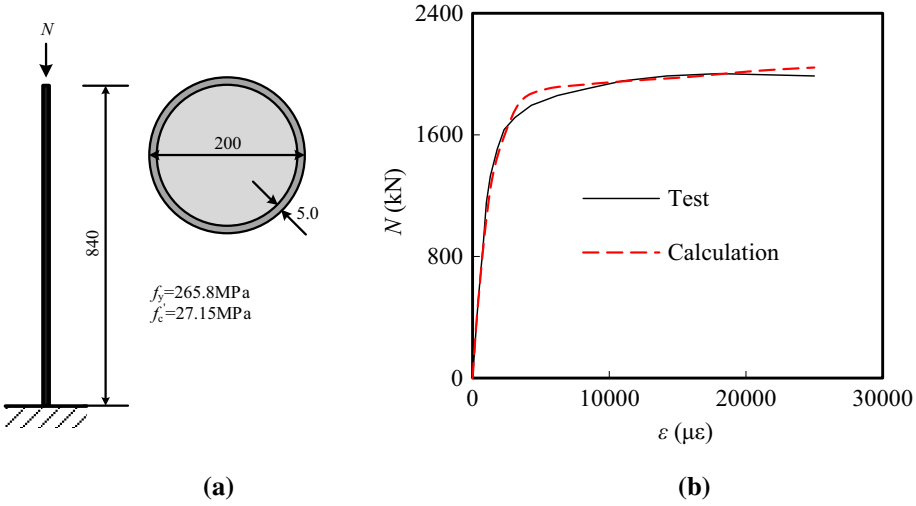

Fig. 16 Verification of CFST column under vertical monotonic load. **a** Information of CFST column, **b** comparison results of CFST column

To verify the iConcre02 model which is applicable to CFST columns with square or rectangular section, a square specimen numbered as S100-1 is selected from a group of CFST columns subjected to cyclic loading tests reported by Han et al. (2004). The geometry, material and loading information of this specimen is illustrated in Fig. 17a. The iConcrete02 model and the iSteel05 model are correspondingly employed by the core concrete and steel tube. Figure 17b shows a comparison between the test and numerical results. With the regard to horizontal force versus displacement, the fiber element model gives very close predictions of the trend of strength and stiffness degradation.

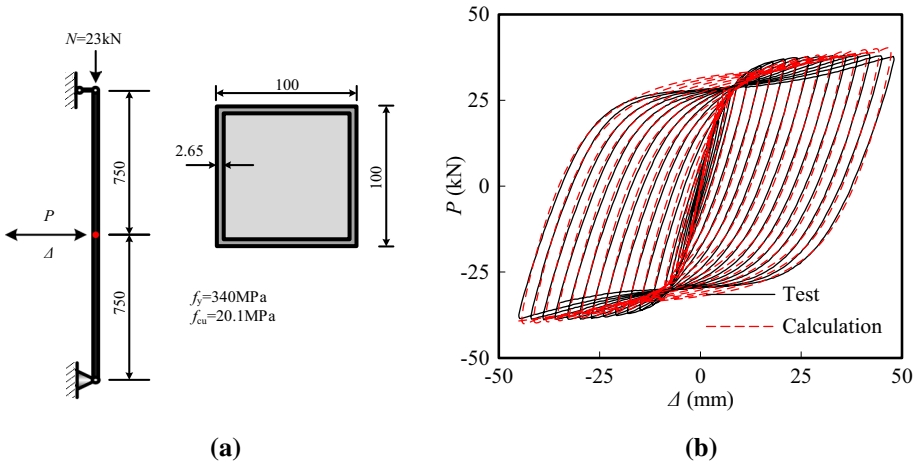

Fig. 17 Verification of CFST column under horizontal cyclic load. **a** Information of CFST column, **b** comparison results of CFST column

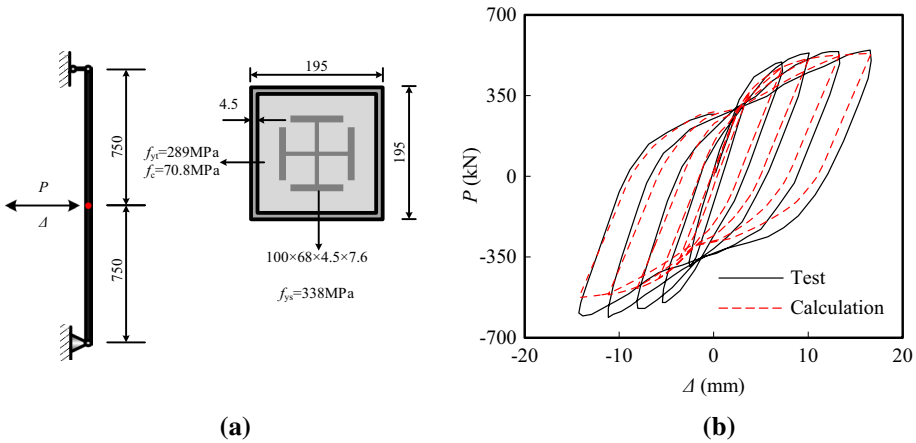

Fig. 18 Verification of steel tubular column filled with steel-reinforced concrete under horizontal cyclic load. **a** Information of steel tubular column filled with steel-reinforced concrete, **b** comparison results of steel tubular column filled with steel-reinforced concrete

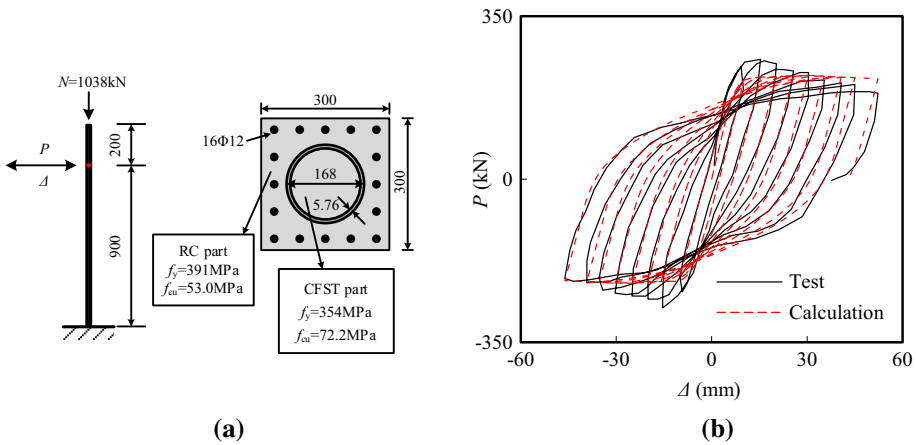

Fig. 19 Verification of CFST composite column under horizontal cyclic load. **a** Information of CFST composite column, **b** comparison results of CFST composite column

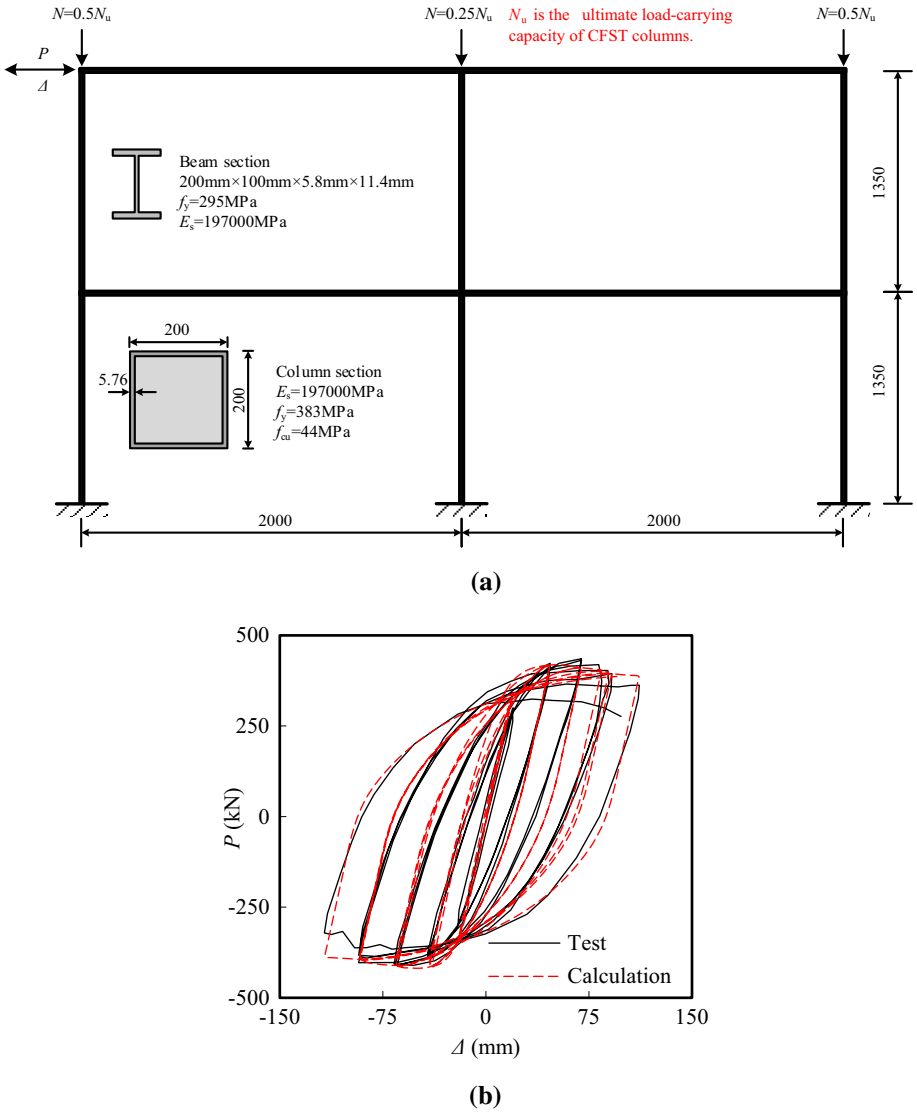

Fig. 20 Verification of composite frame with CFST columns under horizontal cyclic load. **a** Information of composite frame with CFST columns, **b** comparison results of composite frame with CFST columns

Tests on steel tubular columns filled with steel-reinforced high-strength concrete under cyclic loading have been conducted by Zhu et al. (2011). A square section specimen labelled as C4H10-0 is chosen for the verification with its information shown in Fig. 18a. The iConcrete02 model and the iSteel05 model are applied for the core concrete and steel parts (tubes and section steel), respectively. As can be seen in Fig. 18b, close agreement is found between the calculation and test results.

Qian and Kang (2009) studied the seismic performance of a series of composite columns which were formed by embedding a circular CFST column into a square RC column. A specimen CCS1 is selected for verification. The information of this specimen is shown in Fig. 19a. The materials of the outer and core concrete employ the iConcrete03 model and the iConcrete01 model, respectively; while the iSteel03 model is adopted for the steel tube and rebar. The horizontal force and displacement curve simulated by iFiberLUT is shown and compared with the test result in Fig. 19b, where reasonable agreement is observed.

Besides these composite members, steel–concrete composite frames are also selected for verification. Wang et al. (2010) investigated the seismic behavior of a 2-story and 2-bay planar CFST composite frame subjected to horizontal cyclic loading. Figure 20a shows the geometry, material and loading information of this composite frame. The iConcrete01 model and the iSteel03 model are used for the concrete and steel components (steel tubes and beams), respectively. The calculation result gives good agreement with the test result in terms of the relation of the horizontal force and displacement, as shown in Fig. 20b.

Guo et al. (2013) conducted a progressive collapse test of a 4-bay 1/3 scale planar steel–concrete composite frame. The geometry, material and loading information are displayed in Fig. 21a. The steel frame and the concrete slab are simulated

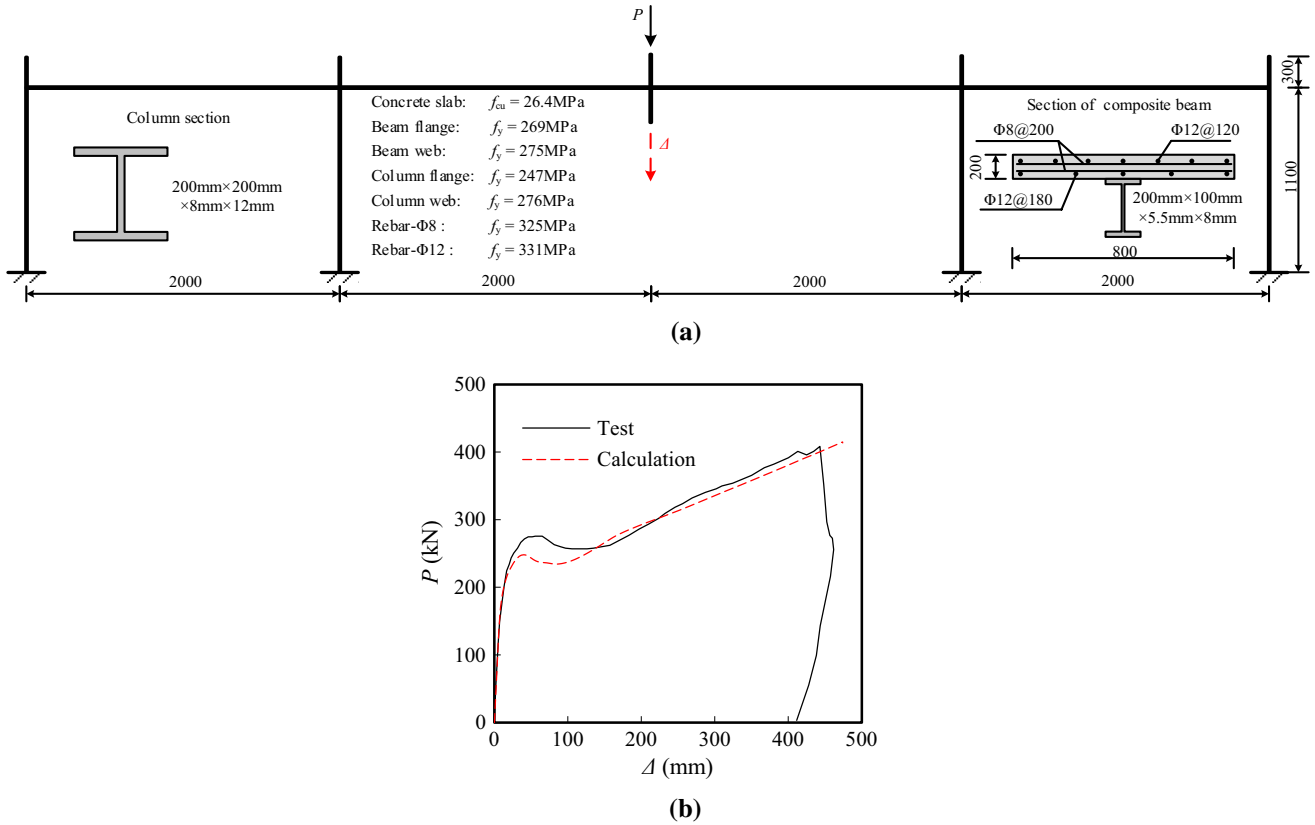

Fig. 21 Verification of steel–concrete composite frame under a column removal scenario. **a** Information of steel–concrete composite frame, **b** comparison results of steel–concrete composite frame

by fiber beam element and multi-layer shell element, respectively. Moreover, the iSteel05 model is used for the steel parts (steel beams, columns and rebar), while the material model for the concrete slab employs the concrete damaged plasticity model in ABAQUS with the stress–strain relation of envelope curve of the iConcrete03 model. The relation of vertical force and middle column displacement specifies the capacity of this composite frame to resist collapse. The comparison between the calculation and test results is illustrated in Fig. 21b. Due to the crack and degradation of concrete slab and fracture of welds in steel frames which cause the failure of this composite frame, certain differences between the simulation and test results can be detected at the failure stage. Nevertheless, the overall behavior is predicted and the collapse-resistant trend of this frame is reasonably similar with the test result.

5 Conclusions

In this study, a fiber model program iFiberLUT which contains an ABAQUS Fiber Generator and a material library is developed based on the secondary development interface of ABAQUS. Several conclusions can be drawn based on the current study:

1. The ABAQUS Fiber Generator can automatically divide beam and column sections into a series of fibers and thus efficiently reduce the modeling workloads. The iFiberLUT material library includes several concrete and steel uniaxial constitutive models. These material models can be used in different types of steel and concrete components and structures under different loadings. Besides, the material library can be extended through the interface sequentially for future studies.
2. The performance of iFiberLUT is validated by a serial of numerical investigations on typical steel, concrete and composite components and frame structures. This program performs a high calculation accuracy and favorable convergence based on the ABAQUS solver.
3. The developed fiber model program is proved to function well in the nonlinear analysis of structures within a wide range of applications. Combining with ABAQUS solver, it can provide an efficient numerical analysis platform to investigate the elastic–plastic behavior of steel, concrete and steel–concrete composite structures.

Acknowledgements This work was supported by the National Natural Science Foundation of China (Nos. 51768038, 51778274, 51468037) and the Science and Technology Support Program of Gansu Province (No. 1604FKCA107). The financial support is highly appreciated.

References

ABAQUS. (2010). *Abaqus user subroutines reference guide*. Vélizy-Villacoublay: Dassault Systems Inc.

Clough, R. W., & Johnston, S. B. (1966). Effect of stiffness degradation on earthquake ductility requirements. In *Proceedings of Japan earthquake engineering symposium*, Japan (pp. 195–198).

CSI. (2006). *Perform-3D nonlinear analysis and performance assessment for 3D structures user guide*. Berkeley: Computer and Structures Inc.

Esmaeily, A., & Xiao, Y. (2005). Behavior of reinforced concrete columns under variable axial loads: analysis. *ACI Structure Journal, 102*(5), 736–744.

Filippou, F. C., Popov, E. P., & Bertero, V. V. (1983). Effects of bond deterioration on hysteretic behavior of reinforced concrete joints. *Report No. EERC 83-19*. California: Earthquake Engineering Research Center, University of California.

GB50010. (2010). *Code for design of concrete structures*. Beijing: China Architecture & Building Press.

Giuffré, A., & Pinto, P. E. (1970). Il comportamento del cemento armato per sollecitazioni cicliche di forte intensità. *Giornale del Genio Civile, 5*(1), 391–408.

Guo, L. H., Gao, S., Fu, F., & Wang, Y. Y. (2013). Experimental study and numerical analysis of progressive collapse resistance of composite frames. *Journal of Constructional Steel Research, 89*(5), 236–251.

Han, L. H., Yao, G. H., & Tao, Z. (2007). Performance of concrete-filled thin-walled steel tubes under pure torsion. *Thin-Walled Structures, 45*(1), 24–36.

Han, L. H., You, J. T., Yang, Y. F., & Tao, Z. (2004). Behavior of concrete-filled steel rectangular hollow sectional columns subjected to cyclic loading. *China Civil Engineer Journal, 37*(11), 11–22.

Hu, H. T., Huang, C. S., Wu, M. H., & Wu, Y. M. (2003). Nonlinear analysis of axially loaded concrete-filled tube columns with confinement effect. *Journal of Structural Engineering, 129*(10), 1322–1329.

Karsan, I. D., & Jirsa, J. O. (1969). Behavior of concrete under compressive loadings. *Journal of the Structural Division, 95*(12), 2543–2564.

Katwal, U., Tao, Z., Hassan, M. K., & Wang, W. D. (2017). Simplified numerical modeling of axially loaded circular concrete-filled steel stub columns. *Journal of Structural Engineering, 143*(12), 0417169.

Kawashima, K., Watanabe, G., & Hayakawa, R. (2004). Seismic performance of RC bridge columns subjected to bilateral excitation. *Journal of Earthquake Engineering, 8*(4), 107–132.

Kent, D. C., & Park, R. (1971). Flexural members with confined concrete. *Journal of the Structural Division, 97*(7), 1969–1990.

Légeron, F., Paultre, P., & Mazar, J. (2005). Damage mechanics modeling of nonlinear seismic behavior of concrete structures. *Journal of Structural Engineering, 131*(6), 946–954.

Lu, X. Z., Lin, X. C., Ma, Y. H., Li, Y., & Ye, L. P. (2008) Numerical simulation for the progressive collapse of concrete building due to earthquake. In *Proceedings of the 14th world conference on earthquake engineering*, Beijing, China.

Lu, X. Z., Ye, L. P., Ma, Y. H., & Tang, D. Y. (2012). Lessons from the collapse of typical RC frames in Xuankou School during the great Wenchuan Earthquake. *Advances in Structural Engineering, 15*(1), 139–153.

Lu, X. Z., Ye, L. P., & Miao, Z. W. (2009). *Elasto-plastic analysis of buildings against earthquake*. Beijing: China Architecture & Building Press.

Mander, J. B., Priestley, M. J. N., & Park, R. (1988). Theoretical stress–strain model for confined concrete. *Journal of Structural Engineering, 114*(8), 1804–1826.

Mazzoni, S., McKenna, F., Scott, M. H., & Fenves, G. L. (2006). The open system for earthquake engineering simulation (OpenSEES) User command-language manual.

Menegotto, M., & Pinto, P. E. (1973). Method of analysis for cyclically loaded R.C. plane frames including changes in geometry and non-elastic behavior of elements under combined normal force and bending. In *Proceedings of IABSE symposium on the resistance and ultimate deformability of structures acted on by well defined repeated loads*, Switzerland (pp. 15–22).

Qian, J. R., & Kang, H. Z. (2009). Experimental study on seismic behavior of high-strength concrete-filled steel tube composite columns. *Journal of Building Structures, 30*(4), 85–93.

Scott, B. D., Park, R., & Priestley, M. J. N. (1982). Stress–strain behavior of concrete confined by overlapping hoops at low and high strain rates. *ACI Structure Journal, 79*(1), 13–27.

Spacone, E., Filippou, F., & Taucer, F. (1996). Fiber beam-column modeling for non-linear analysis of R/C frames: Part I. Formulation. *Journal of Earthquake Engineering and Structural Dynamics, 25*(7), 711–725.

Tao, M. X., & Nie, J. G. (2014). Fiber beam-column model considering slab spatial composite effect for nonlinear analysis of composite frame systems. *Journal of Structural Engineering, 140*(1), 1–12.

Tao, M. X., & Nie, J. G. (2015). Element mesh, section discretization and material hysteretic laws for fiber beam–column elements of composite structural members. *Materials and Structures, 48*(8), 2521–2544.

Taucer, F. F., Spacone, E., & Filippou, F. C. (1991). A fiber beam-column element for seismic response analysis of reinforced concrete structures. *Report No. UCB/EERC-91/17*. Berkeley: Earthquake Engineering Research Center, University of California.

Wang, X. T., Hao, J. P., Zhou, G. G., Zhang, Y., & Ma, Y. S. F. (2010). Experimental research on seismic behavior of two-story two-bay concrete filled square steel tube columns frame. *Journal of Earthquake Engineering and Engineering Vibration, 30*(3), 70–76.

Wang, X. L., Lu, X. Z., & Ye, L. P. (2007). Numerical simulation for the hysteresis behavior of RC columns under cyclic loads. *Engineering Mechanics, 24*(12), 76–81.

Wang, Y. H., Nie, J. G., & Cai, C. S. (2013). Numerical modeling on concrete structures and steel–concrete composite frame structures. *Composites Part B Engineering, 51*(4), 58–67.

Wu, Y., Zhang, Q. L., & Wang, X. F. (2006). Experimental and numerical studies on seismic behavior of steel frame. *Journal of Xi'an University of Architecture and Technology (Natural Science Edition), 38*(4), 486–490.

Yassin, M. H. M. (1994). *Nonlinear analysis of prestressed concrete structures under monotonic and cyclic loads*. Ph.D. Thesis, University of California, Berkeley.

Yi, W. J., He, Q. F., Xiao, Y., & Kunnath, S. K. (2008). Experimental study on progressive collapse-resistant behavior of reinforced concrete frame structures. *ACI Structure Journal, 105*(4), 433–439.

Zhu, M. C., Liu, J. X., & Wang, Q. X. (2011). Experimental study of seismic behavior of square steel tubes filled with steel-reinforced high-strength concrete. *China Civil Engineer Journal, 44*(7), 55–63.

Zou, X., & Zhou, D. Y. (2005). Experimental analysis of 3-story RC frame structures under cyclic load reversals. *Sichuan Building Science, 31*(2), 7–11.